Data-Driven Iterative Learning LQG Control of Axial-Gap 5-DOF Self-Bearing Motor

1st Bo Li
Department of Mechanical Engineering, College of Science and Engineering, Ritsumeikan University,
Kusatsu, Shiga, Japan
Email: rm0215si@ed.ritsumei.ac.jp

2nd Satoshi Ueno, Member IEEE
Department of Mechanical Engineering, College of Science and Engineering, Ritsumeikan University,
Kusatsu, Shiga, Japan
Email: sueno@se.ritsumei.ac.jp

3rd Chengyan Zhao, Member IEEE
Department of Mechanical Engineering, College of Science and Engineering, Ritsumeikan University,
Kusatsu, Shiga, Japan
Email: c-zhao@fc.ritsumei.ac.jp

***Abstract*—This paper studies the displacement control of the tilt-controlling axial-gap self-bearing motor with single stator. We first work out with the state space description for the motor. To design the control strategy, we adopt Linear-Quadratic-Gaussian (LQG) control to design the balance controller. It is known to us that the selection of matrices Q and R are always determined autonomously, which in terms results to less than perfect control performance in real applications. To overcome this situation, we propose an off-line data-based optimizer to replace the matrices selection process by using fruit fly optimization algorithm (FOA). Finally, the effectiveness of our results are verified through the comparison with LQG by simulation experiments.**

***Index Terms*—Axial-gap magnetic self-bearing motor, displacement control, data-driven, iterative learning optimization, LQG, fruit fly algorithm.**

I. Introduction

Magnetic bearing motor has been regraded as a class of high performance actuator for the merits of non-mechanical friction, high efficiency, and high speed request when compared with mechanical bearing motor [1]. Since the magnetic bearing motor can rotate at a very high speed, a plenty of research results can be found in medical care and industry. For example, the artificial heart powered by such kind of motor has been used to supply blood for human [2]. Another real application that the levitation driving rotation speed can be controlled even up to $7600r/min$ [3].

Since the complex structure of original magnetic bearing motor wherein several couples of magnetic bearings are equipped [4], the manufacturing price is high and its application is constrained. To overcome this problem, a new type called *axial-gap self-bearing motor* (ASBM) has been developed to reduce the number of bearings, which in turn leads to a simpler and smaller construction as well as less control difficulty. Compared with traditional magnetic bearing motors, ASBM is combined by a disk motor and an axial magnetic bearing with the inherited two radial magnetic bearings. However, the ASBM can be realized in the form of either electromagnet motro or permanent-magnet motor [5]. Recently, permanent-magnet motors are more popular for its larger capacity on generating electromagnetic power. Moreover, ASBM allows us to create a magnetic field in the air gap, which means that no field excitation winding, zero power dissipation, and easy math modeling [6]. Besides these, with increased demand on miniaturization of equipment [3], high running stability [4, 7], and noise reduction, many efforts has been devoted to developing new control methods [8].

Proportional-Integral-Derivative (PID) control is first used in magnetic bearing motor control, demonstrates a great performance on stable levitation and smooth angular slewing capability even if it is a multiple-input multiple-output linear system [8]. Actually, axial and radial position of the levitated rotor is controlled by currents or voltages along the d-axis and q-axis with a PID feedback loop [9, 10]. The use of linear control methods to nonlinear problems is not very easy to achieve satisfied performance. To efficiently deal with the nonlinear property, disturbance, and uncertainties [11] of the physical equipment, robust sliding mode control, sliding mode control to stabilize the current and speed to the desired target [12]. Another approach of nonlinear control called partial feedback linearization that aims at to reduce the impact of the majority of nonlinear parts of nonlinear model, where the whole model can be combined from building the math model on each coordinates [13]. Beside these, a multi-variable state feedback control with *Karman Filtering* has been proposed to address the problem of model linearization and coils error [14].

However, the studies mentioned above mainly reported the double stator-type permanent magnet motor. To make the structure more streamlined, single stator-type self-bearing motor has been proposed, which exhibits excellent position control and can rotate up to the critical speed by PID control [15]. It is clear that ASBM system is a typical multi-input/output and coupled nonlinear system. Although design the displacement PID controller separately to control the force on each axial works, the coupled dynamics can still give impact on the control performance. Thus, consider the controller design problem as a whole is essential and still an open problem. For these reasons, in this paper, Linear–quadratic–Gaussian (LQG) control is adopted as the main structure of controller design.

In this paper, we first build the state-space model from the original physical dynamics of ASBM, wherein the tilt control currents are selected as the input to control radial displacements and radial rotation angles. Then, LQG is used in designing the state feedback gain for stabilizing the states

on x-axial and y-axial. However, there exists the fact that the manually selected matrices Q and R of the LQG control can affect the result on state feedback, especially when the control object has the high dimensions. In this case, the selecting process based on the input and output data becomes a NP-hardness problems [16] in control system design. To bridge this gap, we design a data-driven optimizer to iterative learning the selecting process of LQG matrices, where there optimizer is designed by fruit fly optimization algorithm (FOA) [17]. as well as against disturbance and noises of the system.

The main contribution can be summarized as follows:

1) Build the controller design model in the form of state space and design the LQG displacement controller.
2) Design a data-based optimizer for off-line selecting the matrices Q and R, which in turn lead to the better performed feedback matrix of LQG controller.

II. Mathematical Model

In this section, we start by introducing the structure of the magnetic bearing motor and its difficulty in displacement control. As the contribution, we propose that the dynamic model can be expressed in state space model.

From the references [4, 5], we know that the displacement of this kind of magnetic motor is determined by the torques on X-Y directions and the corresponding tilt angles. In details, one has the same poles as the motor and is known as motor current, while the other is known as tilt control current and has plus or minus two poles that differ from the motor. Fig. 1 shows the structure of the the single stator ASBM, where six concentrated windings and an iron core are attached to the upper side of the permanent magnetic for generating the forces for keeping the rotor suspended on X-Y axis and the rotational torque on Z-axis. The sensors are equipped for measuring the displacements labeled on Fig. 1.

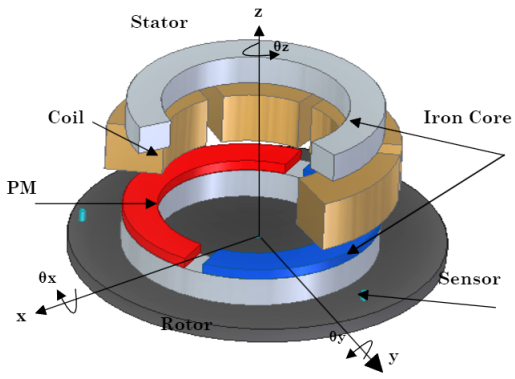

Fig. 1. Structure of a tilt-controlling ASBM

The equivalent current distribution of the rotor magnet is assumed to be sinusoidal, and stator current distribution are

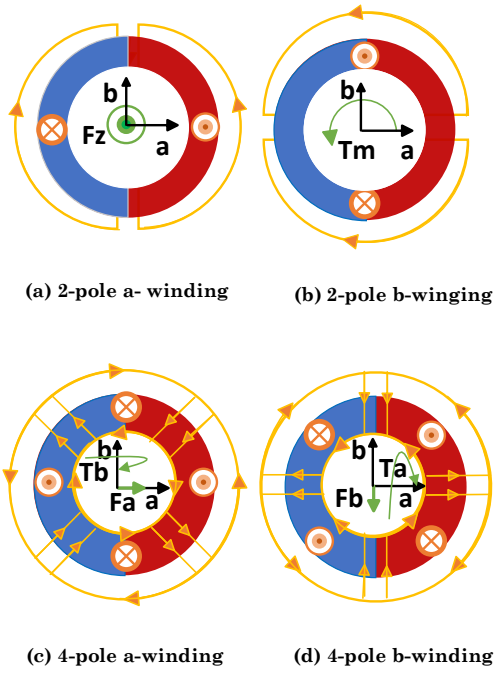

(a) 2-pole a- winding (b) 2-pole b-winging

(c) 4-pole a-winding (d) 4-pole b-winding

Fig. 2. Generation of moments and forces for 2-pole rotor

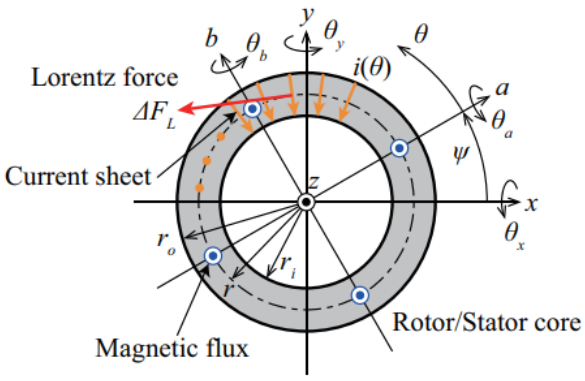

Fig. 3. Top view of rotor

divided into a axis and b axis as shown by Fig. 3. The current on each phase is defined by

$$
\begin{aligned}
i_{Pr}(\theta) &= I_{Pr}\sin\theta \\
i_{Pa}(\theta) &= I_{Pa}\sin\theta \\
i_{Pb}(\theta) &= -I_{Pb}\cos\theta
\end{aligned}
$$

where I_{P*} and θ denote the amplitude and phase of the current. Then, the magnetic flux density distribution by the current can

be expressed as

$$B_{Pr}(\theta) = \frac{4\mu_0 N}{g_0} I_{Pr} \cos\theta$$
$$B_{Pa}(\theta) = \frac{4\mu_0 N}{g_0} I_{Pa} \cos\theta$$
$$B_{Pb}(\theta) = \frac{4\mu_0 N}{g_0} I_{Pb} \sin\theta$$

where μ_0 is the permeability of air, N is equivalent turn number of windings, and g_0 is the air gap between the stator and rotor. Let $B_2(\theta) = B_{2r}(\theta) + B_{2a}(\theta) + B_{2b}(\theta)$ and $B_4(\theta) = B_{4r}(\theta) + B_{4a}(\theta) + B_{4b}(\theta)$, the whole magnetic flux distribution can be shown as $B(\theta) = B_2(\theta) + B_4(\theta)$. Then, the magnetic force of small area ΔS can be expressed as

$$\Delta F_M = \frac{B(\theta)^2}{2\mu_0}\Delta S = \frac{B(\theta)^2}{2\mu_0}\frac{S}{2\pi}d\theta.$$

Therefore, the axial force is expressed as

$$F_z = \frac{4\mu_0 S N^2}{g_0^2}\left((I_{2r}+I_{2a})^2 + I_{2b}^2 + (I_{4r}+I_{4a})^2 + I_{4b}^2\right),$$

where I_{2a}, I_{2b}, and I_{2r} are the currents of a-winding, b-windind and rotor of 2-pole, while I_{4a}, I_{4b}, and I_{4r} are the currents for 4-pole, respectively. Then, the tilt torques can be obtained by

$$T_a = \frac{4\mu_0 r S N^2}{g_0^2}(I_{2r}I_{4b} - I_{4r}I_{2b} + I_{2a}I_{4b} - I_{4a}I_{2b})$$
$$T_b = \frac{4\mu_0 r S N^2}{g_0^2}\left(-(I_{2a}+I_{2r})(I_{4a}+I_{4r}) - I_{2b}I_{4b}\right).$$

Since the motor torque and radial forces are proportional to the Lorentz force, we obtain the magnetic forces

$$T_z = \frac{4\mu_0 S N^2}{g_0}(I_{2r}I_{2b} + 2I_{4r}I_{4b})$$
$$F_a = \frac{3\mu_0 S N^2}{g_{0r}}(I_{2r}I_{4a} - I_{4r}I_{2a} - \frac{I_{2r}I_{4r}}{3} + \frac{I_{2a}I_{4a}}{3} + \frac{I_{2b}I_{4b}}{3})$$
$$F_b = \frac{3\mu_0 S N^2}{g_{0r}}(I_{2r}I_{4b} + I_{4r}I_{2b} + \frac{I_{2a}I_{4b}}{3} - \frac{I_{4a}I_{2b}}{3}).$$

Then, we let axial force current be i_z and motor current be i_m generated in the situation of 2-pole. From Fig. 2 4-pole current generates radial forces and tilt torques. Since the tilt currents i_{ta} and i_{tb} can be seen as intermediate currents, we transform them into the x-y axial by i_{t_x} and i_{t_y}. Then, the transformation is given by

$$\begin{bmatrix} I_{2a} \\ I_{2b} \\ I_{4a} \\ I_{4b} \end{bmatrix} = \begin{bmatrix} 1 & 0 & 0 & 0 \\ 0 & 1 & 0 & 0 \\ 0 & 0 & \sin\psi & -\cos\psi \\ 0 & 0 & \cos\psi & \sin\psi \end{bmatrix} \begin{bmatrix} i_z \\ i_m \\ i_{t_x} \\ i_{t_y} \end{bmatrix}.$$

In reality, I_{2r} is much larger than other currents that it can be ignored. Then, we have

$$F_x \approx -\frac{3\mu_0 S N^2}{g_{0r}}(I_{2r} + \frac{i_{z0}}{3})i_{t_y} \equiv -K_r i_{t_y}$$
$$F_y \approx \frac{3\mu_0 S N^2}{g_{0r}}(I_{2r} + \frac{i_{z0}}{3})i_{t_x} \equiv K_r i_{t_x}$$
$$T_x \approx \frac{4\mu_0 r S N^2}{g_0^2}(I_{2r} + i_{z0})i_{t_x} \equiv K_t i_{t_x}$$
$$T_y \approx \frac{4\mu_0 r S N^2}{g_0^2}(I_{2r} + i_{z0})i_{t_y} \equiv K_t i_{t_y}$$

where i_{z0} is approximated value of forces and torques, K_r is the current stiffness coefficient of F_x and F_y, and K_t is the current stiffness coefficient for T_x and T_y. Let the distance from the center of gravity be z_g. For simplicity, gyroscopic effect are neglected. Thus, the radial motions of 2-pole case can be expressed as

$$\begin{aligned}
m\ddot{x}_1 =& -K_{r_p}x_1 - (K_{r_p}z_g\theta_{x1} + K_r i_{t_y}) \\
m\ddot{x}_2 =& -K_{r_p}x_2 + (K_{r_p}z_g\theta_{x2} + K_r i_{t_x}) \\
I_r\ddot{\theta}_{x1} =& K_{rp}z_g y + (K_{tn} - K_{rp}z_g^2)\theta_{x1} + (K_t - K_r z_g)i_{tx} \\
I_r\ddot{\theta}_{x2} =& -K_{rp}z_g x + (K_{tn} - K_{rp}z_g^2)\theta_{x2} + (K_t - K_r z_g)i_{ty},
\end{aligned} \tag{1}$$

where x_1 and x_2 are the displacement of x-axis and y-axis, respectively. θ_{x1} and θ_{x2} are the tilt angle of x-axis and y-axis. m is the weight of the rotor, I_r is the inertia of radial axis, K_{tn} is negative stiffness for tilt motion, and K_{rp} is passive stiffness for the radial motion. Let the input vector be $u = [i_{t_x}\ i_{t_y}]^\top$, state vector be $x = [x_1\ x_2\ \dot{x}_1\ \dot{x}_2\ \theta_{x1}\ \theta_{x2}\ \dot{\theta}_{x1}\ \dot{\theta}_{x2}]^\top$, and output vector be $y = [x_1\ x_2\ \theta_{x1}\ \theta_{x2}]^\top$, The model introduced in (1) can be formulated in the linear system

$$\begin{cases} \dot{x}(t) = Ax(t) + Bu(t) + v(t) \\ y(t) = Cx(t) + w(t), \end{cases} \tag{2}$$

where the state, input, and output matrix derived from (1) are illustrated as

$$A = \begin{bmatrix}
0 & 0 & 1 & 0 & 0 & 0 & 0 & 0 \\
0 & 0 & 0 & 1 & 0 & 0 & 0 & 0 \\
-\frac{K_{r_p}}{m} & 0 & 0 & 0 & 0 & -\frac{K_{r_p}z_g}{m} & 0 & 0 \\
0 & \frac{K_{r_p}}{m} & 0 & 0 & \frac{K_{r_p}z_g}{m} & 0 & 0 & 0 \\
0 & 0 & 0 & 0 & 0 & 0 & 1 & 0 \\
0 & 0 & 0 & 0 & 0 & 0 & 0 & 1 \\
0 & \frac{K_{r_p}z_g}{I_r} & 0 & 0 & \frac{K_{tn}-K_{r_p}z_g^2}{I_r} & 0 & 0 & 0 \\
-\frac{K_{r_p}z_g}{I_r} & 0 & 0 & 0 & 0 & \frac{K_{tn}-K_{r_p}z_g^2}{I_r} & 0 & 0
\end{bmatrix}$$

$$B^\top = \begin{bmatrix}
0 & 0 & 0 & \frac{K_r}{m} & 0 & 0 & \frac{K_t - K_r z_g}{I_r} & 0 \\
0 & 0 & -\frac{K_r}{m} & 0 & 0 & 0 & 0 & \frac{K_t - K_r z_g}{I_r}
\end{bmatrix}$$

$$C = \begin{bmatrix}
1 & 0 & 0 & 0 & 0 & 0 & 0 & 0 \\
0 & 1 & 0 & 0 & 0 & 0 & 0 & 0 \\
0 & 0 & 0 & 0 & 1 & 0 & 0 & 0 \\
0 & 0 & 0 & 0 & 0 & 1 & 0 & 0
\end{bmatrix}.$$

$v(t)$ and $w(t)$ are the *Gaussian system noise* and *additive white Gaussian measurement noise*, respectively. Since the rank of the controllability matrix of system (2) Rank$[B\ AB\ \dots\ A^{n-1}B] = 8$, the full row rank result allows us to design the LQG controller.

III. Control algorithms design

Following on up from the control target and difficulty introduced in Section II, in this section, we finish the LQG controller for stabilizing the displacement on x-y axis. To resolve the deficiency on manually selecting the Q and R matrices which in turn leads to the negative impact on control performance, we propose a data-driven iterative learning optimizer for efficiently calculating the feedback gain of LQG.

A. LQG control

We start by define performance index of model (2)

$$J = \mathbb{E}\left[\int_0^\infty (x(t)^\top Q x(t) + u(t)^\top R u(t))dt\right] \tag{3}$$

where $\mathbb{E}$ denotes the expected value, and $Q(t)$ and $R(t)$ are weighting coefficients related to state variables and control variables, respectively. The LQG controller that solves the LQG control problem is specified by the following equations:

$$\begin{aligned} &\dot{\hat{x}}(t) = A\hat{x}(t) + Bu(t) + L(t)(y(t) - C\hat{x}(t)),\ \hat{x}(0) = \mathbb{E}[x(0)] \\ &u(t) = -K\hat{x}(t), \end{aligned} \tag{4}$$

where $L(t)$ is called the *Kalman gain* of the associated Kalman filter. Combining the equations (3), (4), and (5), we can obtain the Kalman gain through the following associated matrix Riccati differential equation:

$$\begin{aligned} &\dot{P}(t) = AP(t) + P(t)A^\top - P(t)C^\top W^{-1}(t)CP(t) + v(t) \\ &P(0) = \mathbb{E}[x(0)x^\top(0)]. \end{aligned} \tag{5}$$

Given the solution $P(t)$, the Kalman gain equals

$$L(t) = P(t)C^\top(t)W^{-1}(t).$$

The matrix the feedback gain matrix $K(t)$ is obtained by

$$-\dot{S}(t) = A^\top S(t) + S(t)A - S(t)BR^{-1}B^\top S(t) + Q.$$

Given the solution $S(t)$, the feedback gain equals

$$K(t) = R^{-1}B^\top S(t).$$

B. Data-driven iterative learning optimizer design by FOA

It is well known to us that the feedback gain matrix obtained from LQG depends on the manually selected matrices Q and R. In real application problems, many references have reported that improving the performance by manually selecting Q and R will be an exploded computation. For this reason, we adopt a simple structure but high computing efficiency intelligent optimization method called *fruit fly optimization algorithm* to design an iterative learning optimizer for automatically computing the optimized Q and R. Let i denote the index of the group with the total G generations. We have

$$\begin{aligned} X_i &= X_{axis} + \text{rand}(\dim(X)) \\ Y_i &= Y_{axis} + \text{rand}(\dim(Y)) \\ D_i &= \sqrt{X_i^2 + Y_i^2}, S_i = 1/D_i \\ S_i &= \begin{bmatrix} \lambda_{11} & \lambda_{12} & \cdots & \lambda_{1G} \\ \vdots & \vdots & \cdots & \vdots \\ \lambda_{81} & \lambda_{82} & \cdots & \lambda_{8G} \\ \mu_{11} & \mu_{12} & \cdots & \mu_{1G} \\ \mu_{21} & \mu_{22} & \cdots & \mu_{2G} \end{bmatrix}, \end{aligned} \tag{6}$$

where S_i determines the elements of Q and R and is substituted into the Riccati equation computing the optimized feedback gain. Suppose there exists M groups of fruit fly, j index of iteration of M. Let Δx_j ,Δy_j, $\Delta\theta_{x_j}$, and $\Delta\theta_{y_j}$ be the increments on the state variables, the errors generated in the total iterations were counted by using the standard deviation

$$\begin{aligned} \epsilon_j &= \sqrt{\sum_{j=1}^{G}\Delta x_j^2 + \sum_{j=1}^{G}\Delta y_j^2 + \sum_{j=1}^{G}\theta_{xj}^2 + \sum_{j=1}^{G}\theta_{yj}^2} \\ N &= \sum_{j=1}^{G}(\Delta x_j + \Delta y_j + \Delta\theta_{x_j} + \Delta\theta_{y_j}). \end{aligned}$$

We define that the value of ith fruit fly as S_i,and the average value of all fruit flies can be expressed as

$$x_i = \frac{\sum_{i=1}^{n} S_i}{N}$$

where N is the number of fruit flies. The standard deviation of this group of flies can be expressed as

$$\sigma^2 = \frac{\sum_{i=1}^{n}(S_i - x_i)^2}{N}.$$

When the standard deviation is too high, it indicates that the current result is inadequate and that the step size should be increased to increase the searching speed. Otherwise, when the standard deviation is too small, it indicates that the system is approaching the convergence stage. As a result, the step size should be reduced to prevent premature convergence. On the other hand, keeping the step size in a large range, increases the risk of falling into a local optimum while allowing the results to converge quickly. A step size that is too small will cause the iteration to be very slow. As a result, we define the step size as

$$\ell_{i+1} = \begin{cases} \ell_i + \dfrac{\ln\sigma^2}{N}, & \sigma^2 \geq 1, \\ \ell_i + \dfrac{\ln\sigma^2(N-1)}{N}, & 0.08 \leq \sigma^2 < 1, \\ \ell_i, & 0.01 \leq \sigma^2 < 0.08, \\ \ell_i \tan\dfrac{\pi}{L+6}, & \sigma^2 < 0.01, \end{cases}$$

where ℓ_{i+1} is the $(i+1)$th searching step. However, a random function is used to initialize the first batch of fruit flies,

however after the second time, a different method will be used to update the population's position. The flavour concentration value for each round S_i will depend on the distance of the population to the origin D_i and can be regarded as $S_i = D_i^{-1}$. However S_i is a matrix with high dimensionality and determines the $Q_{i,j}$ and $R_{i,j}$. Then, the Riccati equation in each round of iterations can be expressed as Although we control the parameters of the ith iteration through S_i, it is clear that the underfitting parameters can not necessarily work well for the $(i+1)$th iteration. Thus, in the ith iteration, an adaptive function is used to update the values of the matrix S_i, with the adaptation based on the smallest error value $\epsilon_{i,j}$ of the radial displacements and rotation angles with respect to the coordinate axis. The algorithm is shown as as the following block diagram Fig. 4.

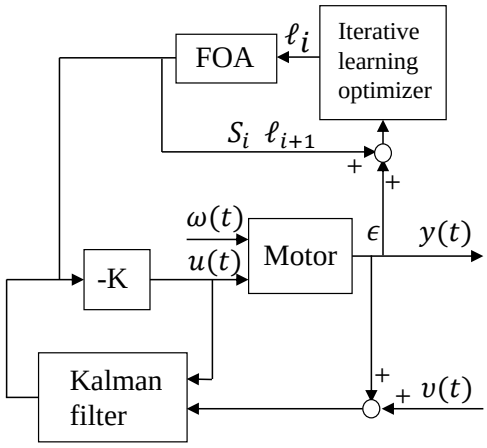

Fig. 4. Block diagram of the data-driven iterative learning based LQG

IV. Simulation experiments

In this section, we verify our proposed results by numerical simulation. Table I illustrates the initialization of the model and FOA algorithm. Fig. 5 shows the trajectories of the optimzation process of the elements on matrices Q and R. To get apparent observations, the initial state is set by $x(0) = [0.5, 0.5, 0, 0, 0.5, 0.5, 0, 0]$. It is clear to see that the values converges to a constant value as the number of iterations G increases. To illustrate the strengths of data-driven learning algorithm over normal LQG, we list the manually selected Q and R matrices as the initialization of data-driven learning algorithm, and the optimization solution is also listed as below:

$$\text{diag}(Q) = [0.94, 0.56, 0.37, 0.68, 0.55, 0.84, 0.21, 1.02]$$
$$\text{diag}(R) = [0.5, 0.7]$$
$$\text{diag}(\bar{Q}) = [0.09, 0.09, 0.16, 0.10, 0.10, 0.81, 0.40, 0.16]$$
$$\text{diag}(\bar{R}) = [0.11, 0.07].$$

Fig. 6 shows the trajectories of the control variables, where the conclusion can be drawn that the data-driven iterative learning based optimizer offers the better parameter matrices Q and R for the LQG feedback gain design.

Algorithm 1 Environmental Selection

Input: Group number M, Initial step size ℓ, last turn of step size ℓ_i, random initial position coordinates X_1, Y_1.
Output: Q, R;

Initialize X_{axis}, Y_{axis}
for $i = 1$; $i \leq M$; $i \leftarrow i + 1$ **do**
  if $i == 1$ **then**
    $X_i = X_{axis} + \text{rand}(\dim(X))$
    $Y_i = Y_{axis} + \text{rand}(\dim(Y))$
  else
    $X_i = X_{axis} + 2\ell_i \times \text{rand}(\dim(X)) - \ell_i$
    $Y_i = Y_{axis} + 2\ell_i \times \text{rand}(\dim(Y)) - \ell_i$
  end if
  $D_i = \sqrt{X_i^2 + Y_i^2}$
  $S_i = 1/D_i$, S_i is affected by the error of the previous population, acting on the next iteration of the population
  Execute iterative learning optimizer
  if then$BestSmell < SmellBest$
    $SmellBest = BestSmall$
    $BestIndex = Index$
  end if
end for
[Q, R]=find($BestIndex$)

Algorithm 2 Iterative Learning Optimizer

Input: Iteration number G, Step size ℓ_i
Output: $BestSmell$, ℓ_{i+1}, N.

for $j = 1$; $j \leq G$; $j \leftarrow j + 1$ **do**
  Update $\Delta x_j, \Delta y_j, \Delta\theta_{xj}, \Delta\theta_{xj}$
  Calculate the error ϵ_j
  $[BestSmell, Index] = \epsilon_j$
  Updating the generation of fruit fly N
  Update the step of next population ℓ_{i+1}
end for

V. Conclusion

In this paper, we first formulate the model where the coupled property of the ASBM is regarded as a whole problem. Since the PID controllers can not well address the coupled state variables, we resort to LQG control as well as handling the noise filtering problem. To optimize and accelerate the process of calculating the selection of Q and R, we proposed a data-driven iterative learning optimizer by FOA. As the future research, the online data-driven algorithms should be investigated, and the real physical experiment ASBM device will be used for verifying the effectiveness on real life cases. Another topic is to apply our results to double-stator ASBM.

Acknowledgement

This work was funded by *Nagamori Foundation 2022* with the project title "Optimal control of 5-DOF self-bearing motor based on data-driven LQG approach".

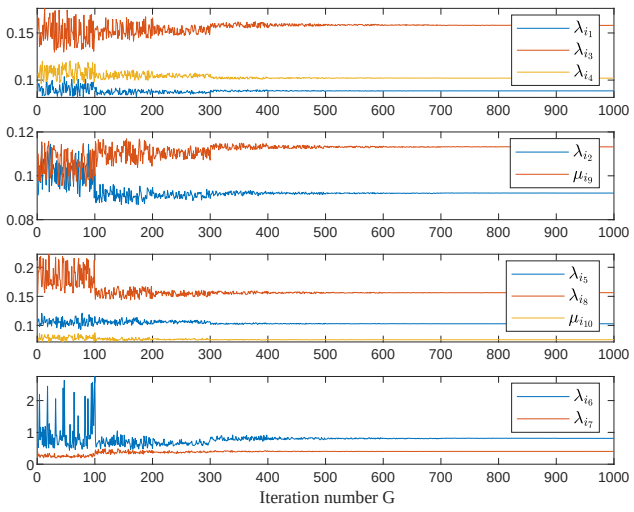

Fig. 5. The evolution process of Q and R versus the iterative learning steps

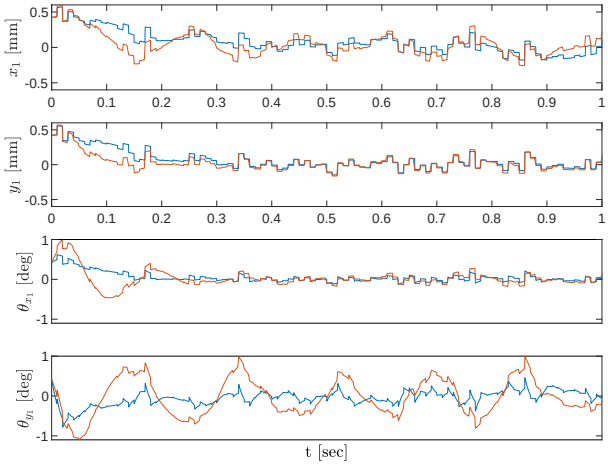

Fig. 6. The results of the displacement y. Red line: LQG. Blue line: data-driven iterative learning based LQG.

TABLE I
PARAMETER USED IN SIMULATION EXPERIMENT.

z_g	-2 [mm]	Center of gravity position
m	0.43 [kg]	Mass of the rotor
k_{rp}	77.9 [N/m]	Passive stiffness (radial)
I_r	470[kgm^2]	Moment of inertia
k_{tn}	1.98×10^6 [N mm/rad]	Negative stiffness for tilt
K_r	1.09 [N/A]	Current stiffness of F_x, F_y
K_t	1.98×10^4[N/A]	Current stiffness of T_x, T_y
G	100	Number of iterations
M	50	Number of population groups
ℓ_i	1	Initial step length
$\sigma^2[w(t)]$	0.4×10^{-4}	Variance of system noise $w(t)$
$\sigma^2[v(t)]$	0.4×10^{-4}	Variance of measured noise $v(t)$

REFERENCES

[1] B. Shafai et al., "Magnetic bearing control systems and adaptive forced balancing," *IEEE Control Systems Magazine*, vol. 14, no. 2, pp. 4–13, 1994.

[2] N. Kurita et al., "A double-sided stator type axial self-bearing motor development for total artificial heart," *IEEE Conf. on Elec. Mach. and Drives,* pp. 1–6, 2017.

[3] Y. Okada et al., "Mixed flow artificial heart pump with axial self-bearing motor," *IEEE/ASME Transactions on Mechatronics*, vol. 10, no. 6, pp. 658–665, 2005.

[4] Q. D. Nguyen et al., "Analysis and control of nonsalient permanent magnet axial gap self-bearing motor," *IEEE Trans. Indus. Elec.*, vol. 58, no. 7, pp. 2644-2652, 2011.

[5] Q. D. Nguyen et al., "Modeling and control of salient-pole permanent magnet axial-gap self-bearing motor," *IEEE Trans. Mech.*, vol. 16, no. 3, pp. 518–526, 2011.

[6] P. Pillay and R. Krishnan, "Modeling of permanent magnet motor drives," *IEEE Transactions on Industrial Electronics,* vol. 35, no. 4, pp. 537–541, 1988.

[7] H. Sugimoto and A. Chiba, "Stability Consideration of Magnetic Suspension in Two-Axis Actively Positioned Bearingless Motor With Collocation Problem," *IEEE Tran. on Ind. Appl.,* vol. 50, no. 1, pp. 338–345, 2014.

[8] Z. Ren "Closed-loop performance of a six degree-of-freedom precision magnetic actuator," *IEEE/ASME Trans. Mechatronics,* vol. 10, no. 6, pp. 666–674, 2005.

[9] M. Osa, "Double stator axial gap type ultracompact 5-DOF controlled selfbearing motor for rotary pediatric ventricular assist device," *IEEE Transactions on Industry Applications,* vol. 57, no. 6, pp. 6744–6753, 2021.

[10] J. V. Verdeghem et al., "Dynamical modeling of passively levitated electrodynamic thrust selfbearing machines," *IEEE Transactions on Industry Applications*, vol. 55, no. 2, pp. 1447–1460, 2019.

[11] S. Ueno et al., "Development of a lorentz-force-type slotless self-bearing motor," *Journal of System Design and Dynamics,* vol. 3, no. 4, pp. 462–470, 2009.

[12] Q. D. Nguyen et al., "Robust sliding mode control-based a novel super-twisting disturbance observer and fixed-time state observer for slotless-self bearing motor system," *IEEE Access*, vol. 10, pp. 23980–23994, 2022.

[13] H. Grabner, "Nonlinear Feedback Control of a Bearingless Brushless DC Motor," *IEEE/ASME Transactions on Mechatronics*, vol. 15, no. 1, pp. 40–47, 2010.

[14] T. Baumgartner and J. W. Kolar, "Multi-variable state feedback control of a 500000-r/min self-bearing permanent-magnet motor," *IEEE/ASME Transactions on Mechatronics*, vol. 20, no. 3, pp. 1149–1159, 2015.

[15] S. Ueno, "Improvement of stability of an tilt-Controlling axial gap self-bearing motor with single stator," in *12th Asian Control Conference,* pp. 1216–1221, 2019.

[16] V. Blondel and J. N. Tsitsiklis, "NP-hardness of some linear control design problems," *SIAM Journal on Control and Optimization,* vol. 35, no. 6, pp. 2118–2127, 1997.

[17] W. T. Pan, "A new Fruit Fly Optimization Algorithm: Taking the financial distress model as an example," *Knowledge-Based Systems*, vol. 26, pp. 69–74, 2012.